NASA TN D-100

TECHNICAL NOTE
D-100

AN ANALYSIS OF INCREMENTAL HORIZONTAL-TAIL LOADS MEASURED ON A SWEPT-WING BOMBER AIRPLANE IN SIDESLIP MANEUVERS

By William A. McGowan

Langley Research Center
Langley Field, Va.

NATIONAL AERONAUTICS AND SPACE ADMINISTRATION

WASHINGTON

October 1959

NATIONAL AERONAUTICS AND SPACE ADMINISTRATION

TECHNICAL NOTE D-100

AN ANALYSIS OF INCREMENTAL HORIZONTAL-TAIL LOADS MEASURED ON A SWEPT-WING BOMBER AIRPLANE IN SIDESLIP MANEUVERS

By William A. McGowan

SUMMARY

Results are presented of an analysis of incremental horizontal-tail loads measured in flight on a swept-wing bomber airplane during rudder-step, aileron-roll, and steady-sideslip maneuvers. The flight tests were made at altitudes of 15,000, 25,000, and 35,000 feet and at Mach numbers from 0.49 to 0.82.

The derivatives of the horizontal-tail normal-force and rolling-moment coefficients with respect to sideslip angle and the derivative of the wing-fuselage pitching-moment coefficient with respect to sideslip angle were derived from the flight measurements. Comparisons of the design horizontal-tail unsymmetrical shear load and the design wing-fuselage pitching-moment derivatives with the respective flight values showed fair agreement. Theoretical and design-specification values of horizontal-tail rolling-moment derivatives were about half the magnitude of the flight values over the altitude and Mach number ranges.

The spanwise center-of-pressure locations for the incremental horizontal-tail loads due to sideslip angle on the leading and trailing horizontal tails were located approximately at the mean aerodynamic chord station during the test maneuvers.

There were no apparent aeroelastic effects on the derivatives obtained from these tests.

INTRODUCTION

The National Aeronautics and Space Administration has carried out a comprehensive flight-test program on a B-47 airplane and, as a result, data were available which enabled an analysis to be made of the incremental horizontal-tail shear and rolling-moment loads measured in sideslip maneuvers.

A need for incremental horizontal-tail-load data on bomber-type aircraft in sideslip was indicated in reference 1. Reference 2 presented flight-test results on a medium bomber airplane that incorporated dihedral in the horizontal tail. This paper presents results of measurements made on a medium bomber airplane with swept horizontal-tail surfaces.

The analysis was made of measurements taken during rudder-step, aileron-roll, and steady-sideslip maneuvers covering a sideslip-angle range of approximately 6° at altitudes of 15,000, 25,000, and 35,000 feet over a Mach number range of 0.49 to 0.82.

The derivatives of the horizontal-tail rolling-moment and unsymmetrical normal-force coefficients with respect to sideslip angle were obtained from the present flight tests and are compared, respectively, with the rolling-moment derivatives calculated by using the methods given in references 3 and 4 and the design unsymmetrical load presented in reference 5.

The derivative of the wing-fuselage pitching-moment coefficient with respect to sideslip angle was evaluated from the incremental horizontal-tail loads measured in steady-sideslip maneuvers and was compared with the wind-tunnel results used in design. (See ref. 5.)

SYMBOLS

$b_h'/2$	semispan of horizontal tail outboard of strain-gage station, in.
b_h	span of horizontal tail, in.
$\left(C_{N_{\lvert\Delta\beta\rvert}}\right)_l$, $\left(C_{N_{\lvert\Delta\beta\rvert}}\right)_t$	derivative of normal-force coefficient with respect to sideslip angle for leading and trailing horizontal tail, respectively, per degree
$\left(C_{l_{\lvert\Delta\beta\rvert}}\right)_l$, $\left(C_{l_{\lvert\Delta\beta\rvert}}\right)_t$	derivative of rolling-moment coefficient with respect to sideslip angle for leading and trailing horizontal tail, respectively, per degree
$C_{m_{\lvert\Delta\beta\rvert}}$	derivative of pitching-moment coefficient with respect to sideslip angle for wing-fuselage combination (about quarter-chord point of $\bar{c}_w$), per degree

$\bar{c}_w$ mean aerodynamic chord of wing, ft

$\bar{c}_h$ mean aerodynamic chord of horizontal tail, ft

c_h section chord of horizontal tail, ft

$\left(C_{N_{|\Delta\beta|}}\right)_{l-t}$ derivative of horizontal-tail unsymmetrical normal-force coefficient with respect to sideslip angle, $\left(C_{N_{|\Delta\beta|}}\right)_l - \left(C_{N_{|\Delta\beta|}}\right)_t$, per degree

$\left(C_{l_{|\Delta\beta|}}\right)_{l-t}$ derivative of total horizontal-tail rolling-moment coefficient with respect to sideslip angle, $\left(C_{l_{|\Delta\beta|}}\right)_l - \left(C_{l_{|\Delta\beta|}}\right)_t$, per degree

l horizontal-tail length, airplane center of gravity to quarter-chord point of $\bar{c}_h$, approximately -46.5 ft

ΔL_l, ΔL_t incremental aerodynamic shear load, outboard of strain-gage station, on leading and trailing horizontal tail, respectively, lb

M Mach number

ΔM_l, ΔM_t incremental aerodynamic rolling moment, outboard of strain-gage station, on leading and trailing horizontal tail, respectively, in-lb

q dynamic pressure, lb/sq ft

S_h' horizontal-tail area outboard of strain-gage stations, sq ft

S_h horizontal-tail area, sq ft

S_w wing area, sq ft

$\Delta\alpha$ effective incremental angle of attack of horizontal tail associated with symmetrical loading, deg

Λ horizontal-tail sweepback angle of quarter-chord line, deg

$|\Delta\beta|$ incremental angle of sideslip at the tail (absolute value), deg

Δp incremental airplane rolling velocity, radians/sec

Incremental quantities (prefixed by Δ) were measured from the trim flight values. Leading horizontal tail was defined as the side of the horizontal tail that was windward in sideslip. Trailing horizontal tail was defined as the side of the horizontal tail that was leeward in sideslip.

APPARATUS AND TESTS

Test Airplane

A swept-wing jet-propelled medium-bomber airplane was used for the tests. (See fig. 1.) Overall dimensions of the test airplane are given in the three-view drawings in figure 2, and other dimensions and characteristics are listed in table I. The plan form of the horizontal tail is shown in figure 3 and the ordinates and a sketch of the airfoil section are shown in table II.

Several minor external modifications were made on the airplane to accommodate some of the instrumentation. External changes include the addition of a nose boom and an optigraph fairing on top of the fuselage located over the wing center section. The yaw damper, although part of the standard equipment, was not used during the present tests.

Instrumentation

Standard NASA instruments were used to record airspeed, altitude, angular velocities, accelerations, and angle of sideslip. A boom extending forward of the fuselage nose, equivalent to a distance of approximately 0.8 of the maximum diameter of the fuselage, housed the airspeed, altitude, angle-of-attack, and angle-of-sideslip sensing devices. The airspeed system was calibrated in flight and the sideslip angle at the airplane tail was obtained by correcting the measured sideslip angle for the effects of the fuselage on the airstream at the sensing vane and for yawing velocity of the airplane. Angular velocities were measured at the approximate airplane center-of-gravity position.

Strain gages located near the root of the horizontal tail (fig. 3) measured structural shears and rolling moments. A strain-gage calibration procedure similar to that outlined in reference 6 was used to combine the primary strain-gage bridges and to obtain equations for structural loads in terms of the gage outputs as recorded on 18-channel oscillographs.

A time pulse of 0.1 second correlated the records of all recording instruments.

Estimated Accuracies

The accuracies of the measured quantities were estimated to be as follows:

Sideslip angle, $\lvert\Delta\beta\rvert$, deg	±0.1
Mach number	±0.01
Horizontal-tail aerodynamic shear load, ΔL_l, ΔL_t, lb	±100
Horizontal-tail aerodynamic rolling moment, ΔM_l, ΔM_t, in-lb	±6,000
Rolling velocity, Δp, radians/sec	±0.003

Test Maneuvers

The flight-test maneuvers analyzed were a series of rudder-step, aileron-roll, and steady-sideslip runs covering a sideslip-angle range of approximately 6° at altitudes of 15,000, 25,000, and 35,000 feet over a Mach number range from 0.49 to 0.82. Characteristics of the flight-test maneuvers analyzed are given in table III. Variations of Reynolds number with Mach number at the three test altitudes are shown in figure 4. Reynolds numbers were based on the horizontal-tail mean aerodynamic chord $\bar{c}_h$.

Maneuvers were initiated with the airplane in the clean configuration (that is, landing gear and flaps up) and trimmed for straight and level flight. Brief descriptions of the three types of maneuvers analyzed are given in reference 7. The center-of-gravity position, airspeed, and altitude remained effectively constant during any particular test run.

Positive directions of the measured quantities are given on a schematic sketch of the airplane in figure 5.

METHOD AND RESULTS

Time histories from typical rudder-step and aileron-roll maneuvers are shown in figures 6 and 7, respectively. The flight records were read at the times shown by the symbols and the various quantities at these times were used directly in the analysis. The aerodynamic loads were obtained by the addition of inertia loads to the measured structural-shear and rolling-moment loads. Cross plots of the horizontal-tail loads and sideslip angles yielded the parameters from which the derivatives with respect to sideslip angle $C_{N_{|\Delta\beta|}}$, $C_{l_{|\Delta\beta|}}$, and $C_{m_{|\Delta\beta|}}$ were derived.

Horizontal-Tail Shear Load

The incremental shear loads on the horizontal tail during each test maneuver were primarily attributed to effective incremental angles of attack caused by (a) changes in air flow about the empennage with sideslip angle, (b) changes in elevator and fuselage deflections and in airplane attitude and pitching velocity, and (c) rolling velocity. The incremental horizontal-tail loads, associated with the incremental angles of attack, were defined: by $\Delta L_{|\Delta\beta|}|\Delta\beta|$, for those associated with flow changes stated in (a); by $\Delta L_{\Delta\alpha}\Delta\alpha$, for those changes of (b); and by $\Delta L_{\Delta p}\Delta p$, for the loads associated with the rolling velocity of (c).

As a first approximation in the analysis, the total incremental aerodynamic shear loads on the leading and trailing horizontal tails were written as

$$\Delta L_l = \left(\Delta L_{|\Delta\beta|}\right)_l |\Delta\beta| + \left(\Delta L_{\Delta\alpha}\right)_l \Delta\alpha + \left(\Delta L_{\Delta p}\right)_l \Delta p$$

and

$$\Delta L_t = \left(\Delta L_{|\Delta\beta|}\right)_t |\Delta\beta| + \left(\Delta L_{\Delta\alpha}\right)_t \Delta\alpha + \left(\Delta L_{\Delta p}\right)_t \Delta p$$

A preliminary investigation indicated that the measured horizontal-tail loads attributed to rolling velocity were relatively small during the test maneuvers. A similar result was reported in reference 7 of loads measured on the vertical tail of the test airplane during the same maneuvers. Hence, the third terms of the equations above were eliminated and in the analysis the total incremental shear loads on the leading and trailing horizontal tails were expressed by

$$\Delta L_l = \left(\Delta L_{|\Delta\beta|}\right)_l |\Delta\beta| + \left(\Delta L_{\Delta\alpha}\right)_l \Delta\alpha \qquad (1)$$

$$\Delta L_t = \left(\Delta L_{|\Delta\beta|}\right)_t |\Delta\beta| + \left(\Delta L_{\Delta\alpha}\right)_t \Delta\alpha \qquad (2)$$

No direct flight measurements were made of $\Delta\alpha$ in equations (1) and (2) and, therefore, direct solutions of the equations for $\left(\Delta L_{|\Delta\beta|}\right)_l$ and $\left(\Delta L_{|\Delta\beta|}\right)_t$ were not practical. Instead a method was employed to evaluate

the loads due to $\Delta\alpha$, $\left(\Delta L_{\Delta\alpha}\right)_l \Delta\alpha$, and $\left(\Delta L_{\Delta\alpha}\right)_t \Delta\alpha$. The total incremental horizontal-tail shear load, the sum of the loads on the leading and trailing surfaces, is written, from equations (1) and (2), as

$$\Delta L_l + \Delta L_t = |\Delta\beta| \left[\left(\Delta L_{|\Delta\beta|}\right)_l + \left(\Delta L_{|\Delta\beta|}\right)_t\right] + \Delta\alpha \left[\left(\Delta L_{\Delta\alpha}\right)_l + \left(\Delta L_{\Delta\alpha}\right)_t\right] \tag{3}$$

Based on the results of a method given in reference 3, as applied to the test airplane, the incremental loads due to sideslip, $\left(\Delta L_{|\Delta\beta|}\right)_l |\Delta\beta|$ and $\left(\Delta L_{|\Delta\beta|}\right)_t |\Delta\beta|$, were considered to be equal in magnitude and acting in opposite directions. Substituting $\left(\Delta L_{|\Delta\beta|}\right)_l |\Delta\beta| = -\left(\Delta L_{|\Delta\beta|}\right)_t |\Delta\beta|$ into equation (3), the total incremental horizontal-tail shear load can then be written as a function of $\Delta\alpha$ alone as

$$\Delta L_l + \Delta L_t = \Delta\alpha \left[\left(\Delta L_{\Delta\alpha}\right)_l + \left(\Delta L_{\Delta\alpha}\right)_t\right] \tag{4}$$

By definition $\Delta\alpha$ is associated with the symmetrical loads on the horizontal tail; therefore,

$$\left(\Delta L_{\Delta\alpha}\right)_l \Delta\alpha = \left(\Delta L_{\Delta\alpha}\right)_t \Delta\alpha \tag{5}$$

Substituting in equation (4) the expressions

$$\Delta L_l + \Delta L_t = 2\left(\Delta L_{\Delta\alpha}\right)_l \Delta\alpha$$

and

$$\Delta L_l + \Delta L_t = 2\left(\Delta L_{\Delta\alpha}\right)_t \Delta\alpha$$

yields

$$\left(\Delta L_{\Delta\alpha}\right)_l \Delta\alpha = \frac{\Delta L_l + \Delta L_t}{2}$$

and

$$\left(\Delta L_{\Delta\alpha}\right)_t \Delta\alpha = \frac{\Delta L_l + \Delta L_t}{2}$$

Equation (1) can now be written as

$$\Delta L_l = \left(\Delta L_{|\Delta\beta|}\right)_l |\Delta\beta| + \frac{\Delta L_l + \Delta L_t}{2}$$

and equation (2) as

$$\Delta L_t = \left(\Delta L_{|\Delta\beta|}\right)_t |\Delta\beta| + \frac{\Delta L_l + \Delta L_t}{2}$$

Hence,

$$\left(\Delta L_{|\Delta\beta|}\right)_l |\Delta\beta| = \frac{\Delta L_l - \Delta L_t}{2} \tag{6}$$

and

$$\left(\Delta L_{|\Delta\beta|}\right)_t |\Delta\beta| = \frac{\Delta L_t - \Delta L_l}{2} \tag{7}$$

The parameters $\left(\Delta L_{|\Delta\beta|}\right)_l$ and $\left(\Delta L_{|\Delta\beta|}\right)_t$ in equations (6) and (7) can be conveniently evaluated. The incremental sideslip angles $|\Delta\beta|$ and shear loads ΔL_l and ΔL_t were measured in flight. The values of the shear-load terms on the right-hand side of equations (6) and (7) at each time the records were read were plotted against the corresponding sideslip angle $|\Delta\beta|$ for each run listed in table III. (See fig. 8 for examples.) The slopes of the faired lines through the data determine the magnitudes of the parameters $\left(\Delta L_{|\Delta\beta|}\right)_l$ and $\left(\Delta L_{|\Delta\beta|}\right)_t$, defined as

$$\left(\Delta L_{|\Delta\beta|}\right)_l = \left(C_{N_{|\Delta\beta|}}\right)_l qS_h' \tag{8}$$

and

$$\left(\Delta L_{|\Delta\beta|}\right)_t = \left(C_{N_{|\Delta\beta|}}\right)_t qS_h' \tag{9}$$

The derivatives of the horizontal-tail normal-force coefficient with respect to sideslip angle, $\left(C_{N_{|\Delta\beta|}}\right)_l$ and $\left(C_{N_{|\Delta\beta|}}\right)_t$ from equations (8) and (9) for the test runs, are shown in figure 9 as a function of Mach number and altitude. Empirical equations were written to represent the data of figure 9 as

$$\left(C_{N_{|\Delta\beta|}}\right)_t = \frac{0.00570}{\sqrt{1 - M^2\cos^2\Lambda}} \qquad (M \leqq 0.70)$$

and

$$\left(C_{N_{|\Delta\beta|}}\right)_t = \frac{0.00373}{\left(\sqrt{1 - M^2\cos^2\Lambda}\right)^3} \qquad (M \geqq 0.70)$$

for the trailing horizontal tail and as

$$\left(C_{N_{|\Delta\beta|}}\right)_l = \frac{-0.00570}{\sqrt{1 - M^2\cos^2\Lambda}} \qquad (M \leqq 0.70)$$

and

$$\left(C_{N_{|\Delta\beta|}}\right)_l = \frac{-0.00373}{\left(\sqrt{1 - M^2\cos^2\Lambda}\right)^3} \qquad (M \geqq 0.70)$$

for the leading horizontal tail. The variations of $C_{N_{|\Delta\beta|}}$ with Mach number as given by these empirical equations are shown in figure 9 with solid lines.

The derivative of the horizontal-tail unsymmetrical normal-force coefficient with respect to sideslip angle $\left(C_{N_{|\Delta\beta|}}\right)_{l-t}$ was defined as the difference between the derivatives of the leading and trailing horizontal-tail normal-force coefficients $\left(C_{N_{|\Delta\beta|}}\right)_l - \left(C_{N_{|\Delta\beta|}}\right)_t$. The unsymmetrical normal-force derivatives are presented in figure 10. The solid line in figure 10, representing the data, was calculated from the empirical equations

$$\left(C_{N_{|\Delta\beta|}}\right)_{l-t} = \frac{-0.01140}{\sqrt{1 - M^2\cos^2\Lambda}} \qquad (M \leqq 0.70)$$

and

$$\left(C_{N|\Delta\beta|}\right)_{l-t} = \frac{-0.00746}{\left(\sqrt{1 - M^2\cos^2\Lambda}\right)^3} \qquad (M \geqq 0.70)$$

The design horizontal-tail unsymmetrical load of reference 5 was reduced to the form $\left(C_{N|\Delta\beta|}\right)_{l-t}$ and is shown in figure 10 for a comparison with the flight-test values.

Horizontal-Tail Rolling Moment

A similar method to the one used in the development of equations (1) and (2) to express the shear loads on the horizontal tails was used in defining the measured rolling moments on the leading and trailing horizontal tails in sideslip as

$$\Delta M_l = \left(\Delta M_{|\Delta\beta|}\right)_l |\Delta\beta| + \left(\Delta M_{\Delta\alpha}\right)_l \Delta\alpha \qquad (10)$$

and

$$\Delta M_t = \left(\Delta M_{|\Delta\beta|}\right)_t |\Delta\beta| + \left(\Delta M_{\Delta\alpha}\right)_t \Delta\alpha \qquad (11)$$

If steps paralleling those used to write equations (6) and (7) are followed, the incremental rolling moments on the leading and trailing horizontal tails dependent upon sideslip angle were written as

$$\left(\Delta M_{|\Delta\beta|}\right)_l |\Delta\beta| = \frac{\Delta M_l - \Delta M_t}{2} \qquad (12)$$

and

$$\left(\Delta M_{|\Delta\beta|}\right)_t |\Delta\beta| = \frac{\Delta M_t - \Delta M_l}{2} \qquad (13)$$

The leading and trailing horizontal-tail rolling moments per degree sideslip angle were evaluated for each run from measured flight data similar to the examples shown in figure 11; the slopes of the faired lines through the data being a measure of the parameters $\left(\Delta M_{|\Delta\beta|}\right)_l$ and $\left(\Delta M_{|\Delta\beta|}\right)_t$.

By defining

$$\left(\Delta M_{|\Delta\beta|}\right)_l = \left(C_{l_{|\Delta\beta|}}\right)_l qS_h'b_h'$$

and

$$\left(\Delta M_{|\Delta\beta|}\right)_t = \left(C_{l_{|\Delta\beta|}}\right)_t qS_h'b_h'$$

and transposing the known quantities to the right-hand side of the equations as

$$\left(C_{l_{|\Delta\beta|}}\right)_l = \frac{\left(\Delta M_{|\Delta\beta|}\right)_l}{qS_h'b_h'} \tag{14}$$

and

$$\left(C_{l_{|\Delta\beta|}}\right)_t = \frac{\left(\Delta M_{|\Delta\beta|}\right)_t}{qS_h'b_h'} \tag{15}$$

the derivatives of the rolling-moment coefficient with respect to sideslip angle for the leading and trailing horizontal-tail surfaces were evaluated. The rolling-moment derivatives are plotted in figure 12 for each run listed in table III.

The rolling-moment derivatives of the total horizontal tail $\left(C_{l_{|\Delta\beta|}}\right)_{l-t}$ for the test runs are plotted in figure 13 in addition to derivatives developed from the theory of reference 3 and the alternate design specifications of reference 4. The solid line in figure 13, representing the flight data, was calculated from the empirical equations

$$\left(C_{l_{|\Delta\beta|}}\right)_{l-t} = \frac{-0.00242}{\sqrt{1 - M^2\cos^2\Lambda}} \qquad (M \leqq 0.70)$$

and

$$\left(C_{l_{|\Delta\beta|}}\right)_{l-t} = \frac{-0.00159}{\left(\sqrt{1 - M^2\cos^2\Lambda}\right)^3} \qquad (M \geqq 0.70)$$

Negative values of the derivatives indicate rolling-moment directions that tend to turn the leading-tail surface down.

Spanwise Center of Pressure

The center of pressure of the incremental horizontal-tail load due to sideslip angle was located, in percent semispan, from the relationship between the previously determined normal-force and rolling-moment derivatives by

$$\frac{\Delta M_l}{\Delta L_l \frac{b_h}{2}} = \frac{\left(C_{l_{|\Delta\beta|}}\right)_l |\Delta\beta| \, qS_h b_h}{\left(C_{N_{|\Delta\beta|}}\right)_l |\Delta\beta| \, qS_h \frac{b_h}{2}} = 2\frac{\left(C_{l_{|\Delta\beta|}}\right)_l}{\left(C_{N_{|\Delta\beta|}}\right)_l} \tag{16}$$

for the leading surface and for the trailing surface by

$$\frac{\Delta M_t}{\Delta L_t \frac{b_h}{2}} = \frac{\left(C_{l_{|\Delta\beta|}}\right)_t |\Delta\beta| \, qS_h b_h}{\left(C_{N_{|\Delta\beta|}}\right)_t |\Delta\beta| \, qS_h \frac{b_h}{2}} = 2\frac{\left(C_{l_{|\Delta\beta|}}\right)_t}{\left(C_{N_{|\Delta\beta|}}\right)_t} \tag{17}$$

The spanwise center-of-pressure locations of the measured incremental horizontal-tail loads over the Mach number and altitude ranges are shown in figure 14.

Wing-Fuselage Pitching Moment

The wing-fuselage pitching-moment change due to sideslip angle was defined as being proportional to the total incremental horizontal-tail load required to maintain zero airplane pitching moment in steady-sideslip maneuvers.

The summation of pitching moments about the wing mean aerodynamic quarter-chord point $\bar{c}_w/4$ with the airplane in steady sideslip is

$$\left(\Delta L_l + \Delta L_t\right) l + C_{m_{|\Delta\beta|}} |\Delta\beta| \, qS_w \bar{c}_w = 0$$

The wing-fuselage pitching-moment derivative with respect to sideslip angle is, therefore,

$$C_{m_{|\Delta\beta|}} = -\frac{\Delta L_l + \Delta L_t}{|\Delta\beta|} \frac{l}{qS_w \bar{c}_w} \tag{18}$$

The terms on the right-hand side of equation (18) are either measured in flight or obtainable from the airplane geometric characteristics. (See table I.) The $\frac{\Delta L_l + \Delta L_t}{|\Delta\beta|}$ term was evaluated by obtaining the slope of the curve faired through plots of $\Delta L_l + \Delta L_t$ against $|\Delta\beta|$. (See for example, fig. 15.)

The wing-fuselage pitching-moment derivatives for the groups of steady-sideslip runs listed in table III are given in figure 16 as functions of Mach number and altitude. These derivatives in addition to wind-tunnel results used in design (ref. 5) are plotted in figure 17 against airplane tail-off lift coefficient. A positive value of $C_{m_{|\Delta\beta|}}$ indicates a pitchup direction.

DISCUSSION

The incremental shear and rolling-moment loads (eqs. 6, 7, 12, 13, and 18) for the dynamic (rudder-step, and aileron-roll) and quasi-static (steady-sideslip) maneuvers are practically linearly dependent upon sideslip angle. (See figs. 8, 11, and 15.) The leading horizontal-tail surface experienced a down incremental shear loading with sideslip angle and the trailing surface, and up loading.

Because of the assumptions in the method used in the reduction of the flight measurements, the incremental leading and trailing horizontal-tail loads attributed to sideslip angle are equal in magnitude and opposite in sign. The parameters $\Delta L_{|\Delta\beta|}$ and $\Delta M_{|\Delta\beta|}$ as well as the derivatives $C_{N_{|\Delta\beta|}}$ and $C_{l_{|\Delta\beta|}}$ are therefore equal in magnitude and opposite in sign for the leading and trailing horizontal tails.

Horizontal-Tail Normal-Force Derivative

The derivative of the horizontal-tail normal-force coefficient with respect to sideslip angle $C_{N_{|\Delta\beta|}}$ increased in magnitude with Mach number. (See fig. 9.) Aeroelastic effects, if any, at constant Mach number are not apparent because of the scatter of the data.

A similarity exists between the lift-curve slope per degree horizontal-tail angle of attack presented in reference 8 for the test airplane and the $C_{N_{|\Delta\beta|}}$ derivative of the present analysis. That is,

the absolute magnitude of $C_{N_{|\Delta\beta|}}$ over the test Mach number range is approximately one-tenth the value of the lift-curve slope per degree horizontal-tail angle of attack reported in the reference.

The derivative of the horizontal-tail unsymmetrical normal-force coefficient with respect to sideslip angle $\left(C_{N_{|\Delta\beta|}}\right)_{l-t}$, indicating the shear magnitude at the tail center section, increases with Mach number and again aeroelastic effects at constant Mach number, if any, were not apparent because of the scatter in the data. (See fig. 10.) The design horizontal-tail unsymmetrical normal-force derivatives were about 1.2 times the flight-test values at a Mach number of 0.49 and about 0.8 times the flight-test values at a Mach number of 0.82. There was agreement at a Mach number of approximately 0.75 between the flight-test and design values of $\left(C_{N_{|\Delta\beta|}}\right)_{l-t}$.

Horizontal-Tail Rolling-Moment Derivative

The derivative of the horizontal-tail rolling-moment coefficient with respect to sideslip angle (fig. 12) from the flight tests increased in magnitude with Mach number. Aeroelastic effects were not apparent at constant Mach number.

The total horizontal-tail rolling-moment derivative $\left(C_{l_{|\Delta\beta|}}\right)_{l-t}$ (fig. 13) indicates that the rolling-moment derivative tends to turn the leading horizontal tail down. The flight-test derivatives are about twice the magnitude of the derivatives calculated by the methods of reference 3 (theory) and reference 4 (design criteria).

Spanwise Center of Pressure

The center of pressure of the incremental loads due to sideslip angle on the leading and trailing horizontal tails remained approximately at the mean aerodynamic chord location over the test Mach number and altitude ranges.

Horizontal-Tail Pitching-Moment Derivative

The values of the rate of change of pitching-moment coefficient of the wing-fuselage combination with sideslip angle generally indicate a pitchup tendency and are scattered about a faired value of approximately $C_{M_{|\Delta\beta|}} = 0.002$ over the Mach number range. (See fig. 16.) In the

comparison with wind-tunnel results used in design, the pitching-moment derivatives from the flight tests are on the order of magnitude of the wind-tunnel values and show a neutral-stability point in pitch with sideslip angle at a wing-fuselage lift coefficient of about 0.54. (See fig. 17.)

CONCLUSIONS

Results are presented of an analysis of incremental horizontal-tail loads measured in flight on a swept-wing bomber airplane during rudder-step, aileron-roll, and steady-sideslip maneuvers. The flight tests were made at altitudes of 15,000, 25,000, and 35,000 feet and at Mach numbers from 0.49 to 0.82. From the analysis and flight tests the following conclusions may be made:

1. During the test maneuvers the leading horizontal-tail surface experienced a down incremental shear loading with sideslip angle and the trailing surface, an up loading. The derivative of the horizontal-tail normal-force coefficient with respect to sideslip angle increased with Mach number and the trend was represented with Glauert-type functions.

2. The derivative of the horizontal-tail unsymmetrical normal-force coefficient with respect to sideslip angle, obtained from the flight measurements, increased with Mach number. The derivative of the horizontal-tail unsymmetrical normal-force coefficient with respect to sideslip angle obtained from the design unsymmetrical horizontal-tail loads at the design conditions of maximum sideslip angle was equal to the flight value at a Mach number of about 0.75 and was in fair agreement at the other test Mach numbers.

3. The derivative of the horizontal-tail rolling-moment coefficient with respect to sideslip angle indicated a moment direction that would tend to turn the leading surface down. The derivative increased with Mach number and the trend was represented with Glauert-type functions. The rolling-moment derivatives calculated from theory and design specifications were approximately half the flight values over the Mach number range.

4. Spanwise centers of pressure of the incremental horizontal-tail loads attributed to sideslip angle were located approximately at the mean aerodynamic chord station during the test maneuvers.

5. Flight values of the rate of change of pitching-moment coefficient of the wing-fuselage combination with sideslip angle generally indicated a pitchup tendency and were in fair agreement with wind-tunnel results

used in design. Derivatives from the flight-data analysis did not show any aeroelastic effects at constant Mach number.

Langley Research Center,
National Aeronautics and Space Administration,
Langley Field, Va., July 13, 1959.

REFERENCES

1. Pearson, Henry A., McGowan, William A., and Donegan, James J.: Horizontal Tail Loads in Maneuvering Flight. NACA Rep. 1007, 1951. (Supersedes NACA TN 2078.)

2. Cooney, T. V.: The Unsymmetrical Load and Bending Moment on the Horizontal Tail of a Jet-Powered Bomber Measured in Sideslipping Flight. NACA RM L51J24, 1952.

3. Braun, Winfried: Asymmetric Tailplane Loads Due to Sideslip. C.P. No. 119, British A.R.C., 1953.

4. Anon.: Military Specification - Airplane Strength and Rigidity. Military Specification, MIL-A-8629(AER), Aug. 28, 1953.

5. Gray, E. Z., Sandoz, P., and Entz, H.: Design Load Criteria. (Model B-47B) Vol. I. Document No. D-9441 (Contract No. W33-038 ac-22413), Boeing Airplane Co., Nov. 9, 1948.

6. Skopinski, T. H., Aiken, William S., Jr., and Huston, Wilber B.: Calibration of Strain-Gage Installations in Aircraft Structures for the Measurement of Flight Loads. NACA Rep. 1178, 1954. (Supersedes NACA TN 2993.)

7. McGowan, William A., and Cooney, T. V.: An Analysis of Vertical-Tail Loads Measured in Flight on a Swept-Wing Bomber Airplane. NACA RM L57B19, 1957.

8. Aiken, William S., Jr., and Fisher, Raymond A.: Horizontal-Tail Parameters as Determined from Flight-Test Tail Loads on a Flexible Swept-Wing Jet Bomber. NACA RM L56J02, 1957.

TABLE I.- DIMENSIONS AND CHARACTERISTICS OF THE TEST AIRPLANE

Wing:	
Span, ft	116.0
Area, sq ft	1,428.0
Aspect ratio	9.43
Taper ratio	0.42
Thickness ratio	0.12
Mean aerodynamic chord, in.	155.9
Sweep at 25-percent chord, deg	35.0
Root chord, in.	208.0
Tip chord, in.	87.0
Airfoil section	BAC 145
Incidence (root and tip), deg	2.75
Dihedral, deg	0
Horizontal tail:	
Span, ft	33.0
Area, sq ft	268
Area (outboard of strain-gage station on one side), sq ft	115.6
Aspect ratio	4.06
Taper ratio	0.42
Thickness ratio	0.10
Mean aerodynamic chord, in.	102.9
Sweep at 25-percent chord, deg	33.0
Root chord, in.	137.0
Tip chord, in.	58.0
Incidence, deg	-0.25
Airfoil section	BAC 100
Vertical tail:	
Span, ft	18.9
Area (including dorsal), sq ft	230.0
Aspect ratio	1.55
Taper ratio	0.34
Thickness ratio	0.10
Mean aerodynamic chord, in.	158.4
Sweep at 25-percent chord, deg	35.0
Root chord, in.	216.0
Tip chord, in.	74
Airfoil section	BAC 100

Power plant:
Six General Electric J-47-GE-23 turbojet engines with a static sea-level military thrust rating of 5,800 pounds for each engine.

TABLE II.- AIRFOIL ORDINATES OF HORIZONTAL TAIL

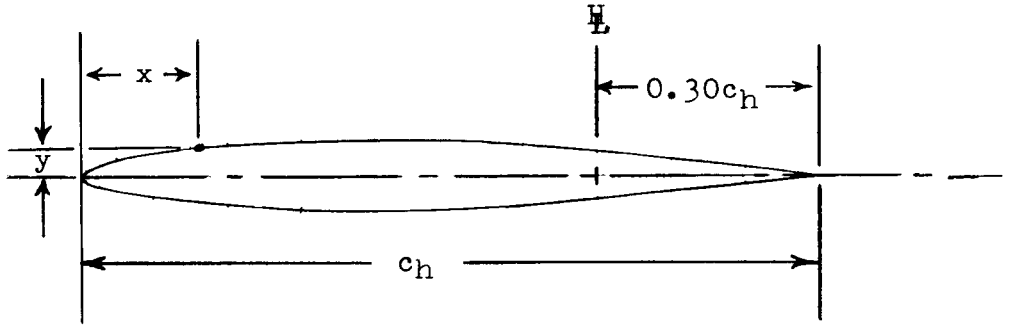

x, percent c_h	± y, percent c_h	x, percent c_h	± y, percent c_h
0	0	25.00	4.51
.50	.78	30.00	4.76
.75	.92	35.00	4.93
1.25	1.16	40.00	5.00
2.50	1.56	50.00	4.80
5.00	2.17	60.00	4.12
7.50	2.64	70.00	3.14
10.00	3.04	80.00	2.10
15.00	3.67	90.00	1.05
20.00	4.15	100.00	0

Airfoil section: 10-percent-thick BAC 100 section similar in cross section to the NASA 65-010 airfoil section modified with straight trailing edges rearward of the 66.5-percent chord.

TABLE III.- CHARACTERISTICS OF THE FLIGHT-TEST MANEUVERS ANALYZED

Flight	Run	Type of maneuver	Altitude, ft	Mach number	Airplane weight, lb	Center of gravity, percent of $\bar{c}_w$
24	10	Right rudder step	34,400	0.60	110,000	23.3
24	16	Right rudder step	35,100	.66	109,000	22.8
24	22	Right rudder step	35,400	.71	108,000	23.9
24	27	Right rudder step	35,800	.77	108,000	22.8
24	32	Right rudder step	35,800	.82	107,000	22.8
24	41	Right rudder step	25,500	.65	104,000	23.8
24	9	Right aileron roll	34,600	.61	110,000	23.2
24	14	Right aileron roll	34,300	.66	109,000	22.9
24	21	Right aileron roll	35,000	.72	109,000	22.9
24	26	Right aileron roll	35,700	.77	108,000	23.0
24	31	Right aileron roll	35,400	.82	107,000	22.6
24	39	Right aileron roll	24,900	.66	105,000	23.3
26	8	Right aileron roll	24,900	.76	115,000	21.1
26	10	Right aileron roll	25,000	.70	115,000	21.1
26	16	Right aileron roll	24,700	.65	113,000	20.5
26	17	Right aileron roll	24,700	.60	113,000	20.2
26	23	Right aileron roll	24,700	.55	112,000	20.5
26	29	Right aileron roll	24,700	.49	111,000	19.8
26	31	Right aileron roll	15,000	.59	110,000	19.6
27	37	Right aileron roll	14,700	.49	105,000	21.0
27	38	Right aileron roll	14,600	.70	105,000	20.8
24	11, 12, and 13	Left steady sideslip	34,000	.59	110,000	23.2
24	18, 19, and 20	Left steady sideslip	35,400	.66	109,000	22.9
24	23, 24, and 25	Left steady sideslip	35,900	.72	108,000	22.9
24	28, 29, and 30	Left steady sideslip	36,000	.77	108,000	22.8
24	33, 34, and 35	Left steady sideslip	37,500	.81	107,000	22.6
24	43, 44, and 45	Left steady sideslip	25,400	.66	104,000	24.2
26	11, 12, 13, and 14	Left steady sideslip	25,800	.70	114,000	20.5
26	18, 19, 20, and 21	Left steady sideslip	25,000	.60	112,000	20.6
26	24, 25, 26, and 27	Left steady sideslip	24,900	.54	111,000	19.9
26	33, 34, and 35	Left steady sideslip	15,500	.59	109,000	19.4
27	13, 14, 15, and 16	Left steady sideslip	24,700	.49	109,000	21.6
27	17, 18, 19, and 20	Left steady sideslip	25,100	.55	109,000	21.7
27	27, 28, 29, and 30	Left steady sideslip	25,700	.70	108,000	21.0
27	31, 32, 33, and 34	Left steady sideslip	25,600	.76	107,000	21.0
28	6, 7, 8, 9, and 10	Left steady sideslip	34,700	.71	117,000	21.9
28	16, 17, 18, 19, and 20	Left steady sideslip	34,900	.81	116,000	21.7

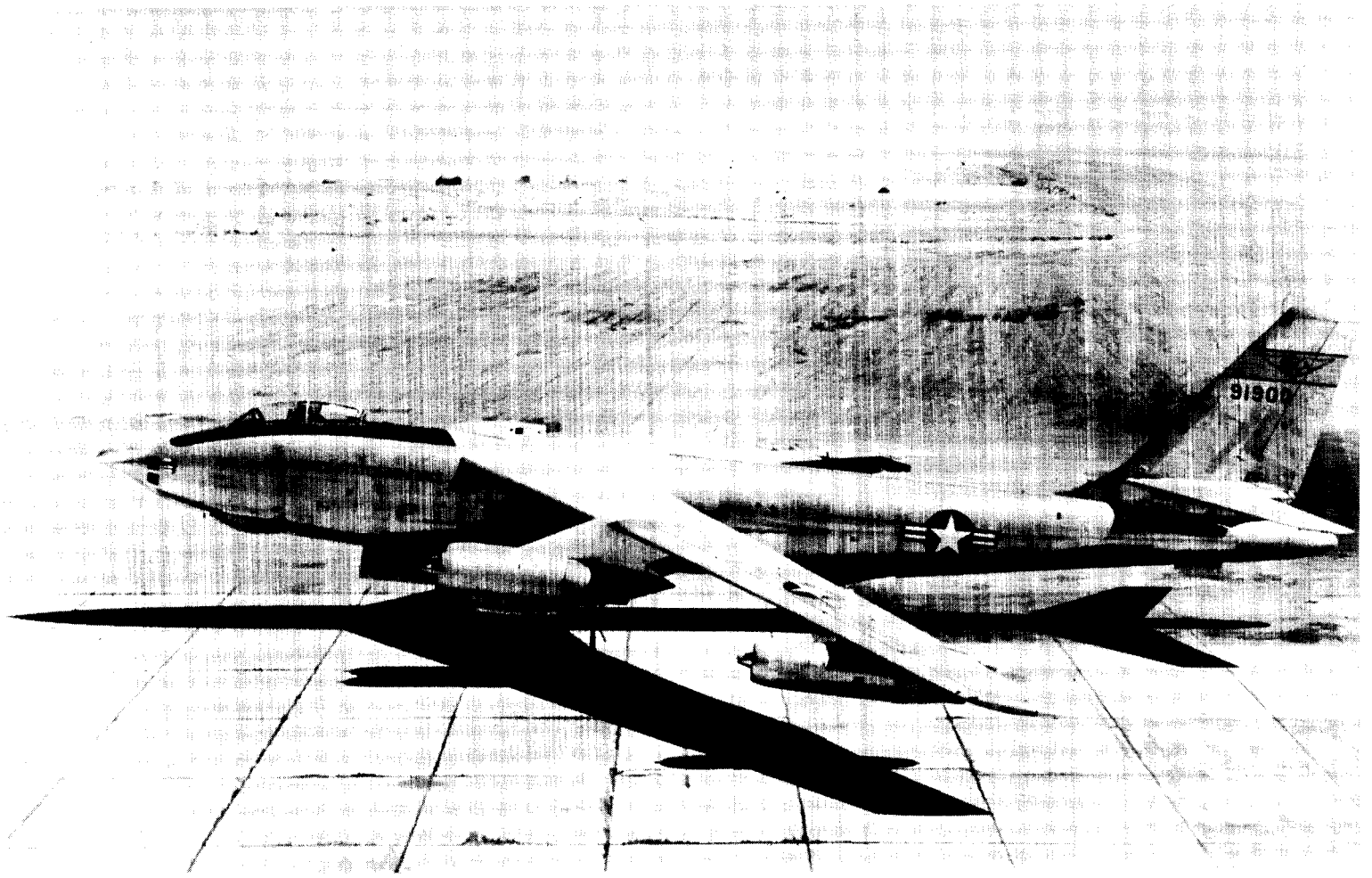

Figure 1.- Test airplane. L-86692

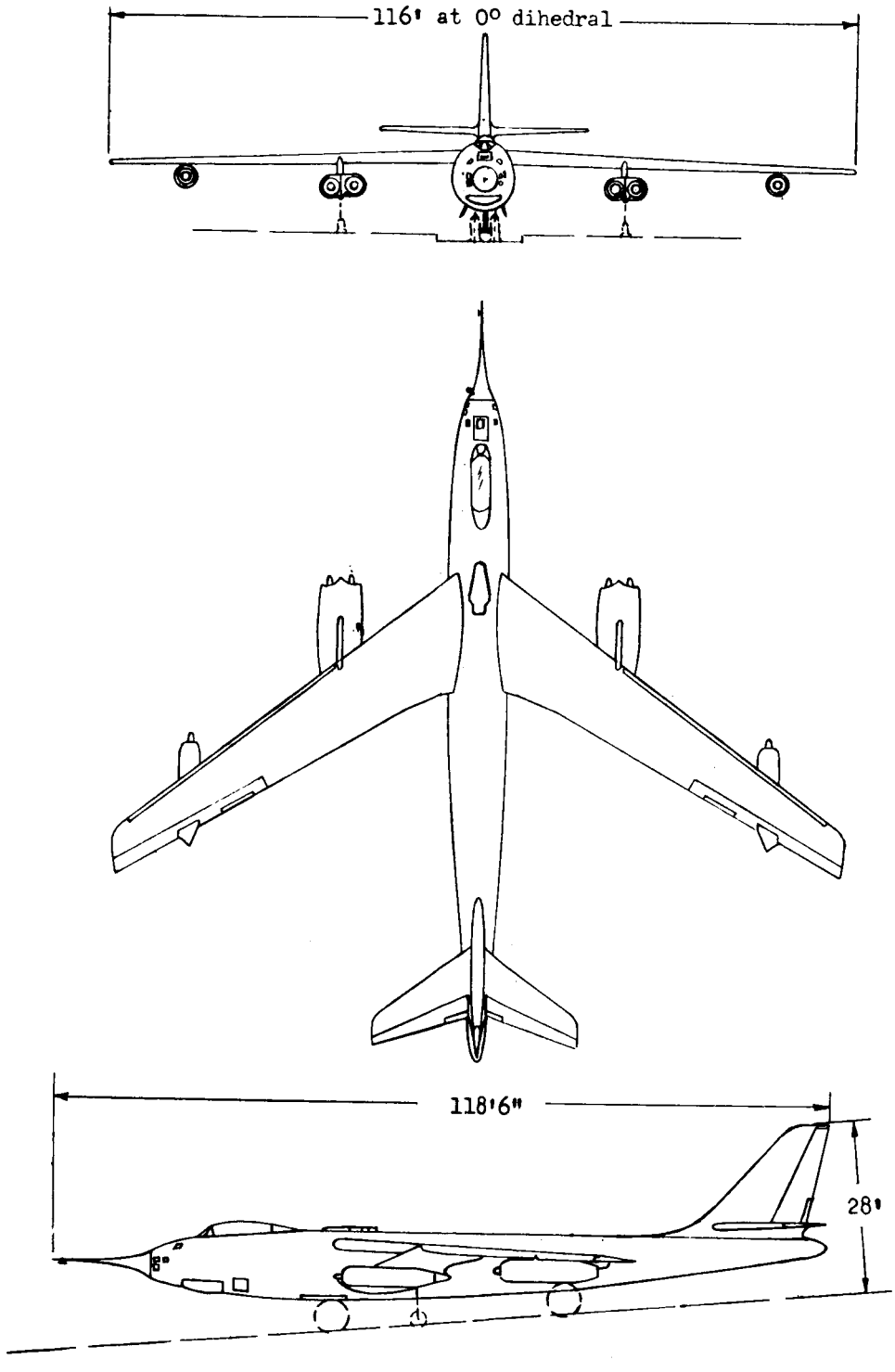

Figure 2.- Principal dimensions of the test airplane.

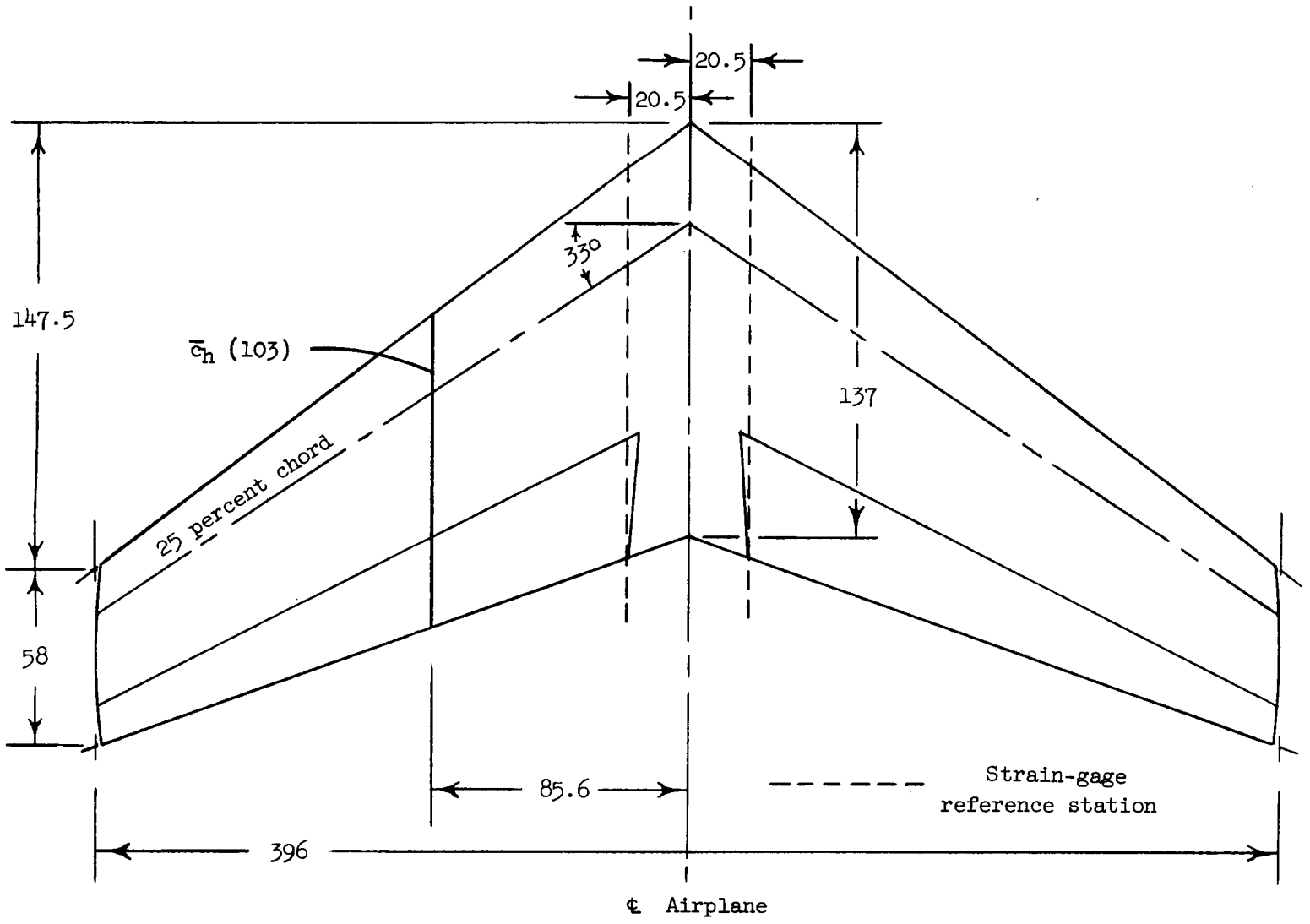

Figure 3.- Horizontal tail. All dimensions are in inches.

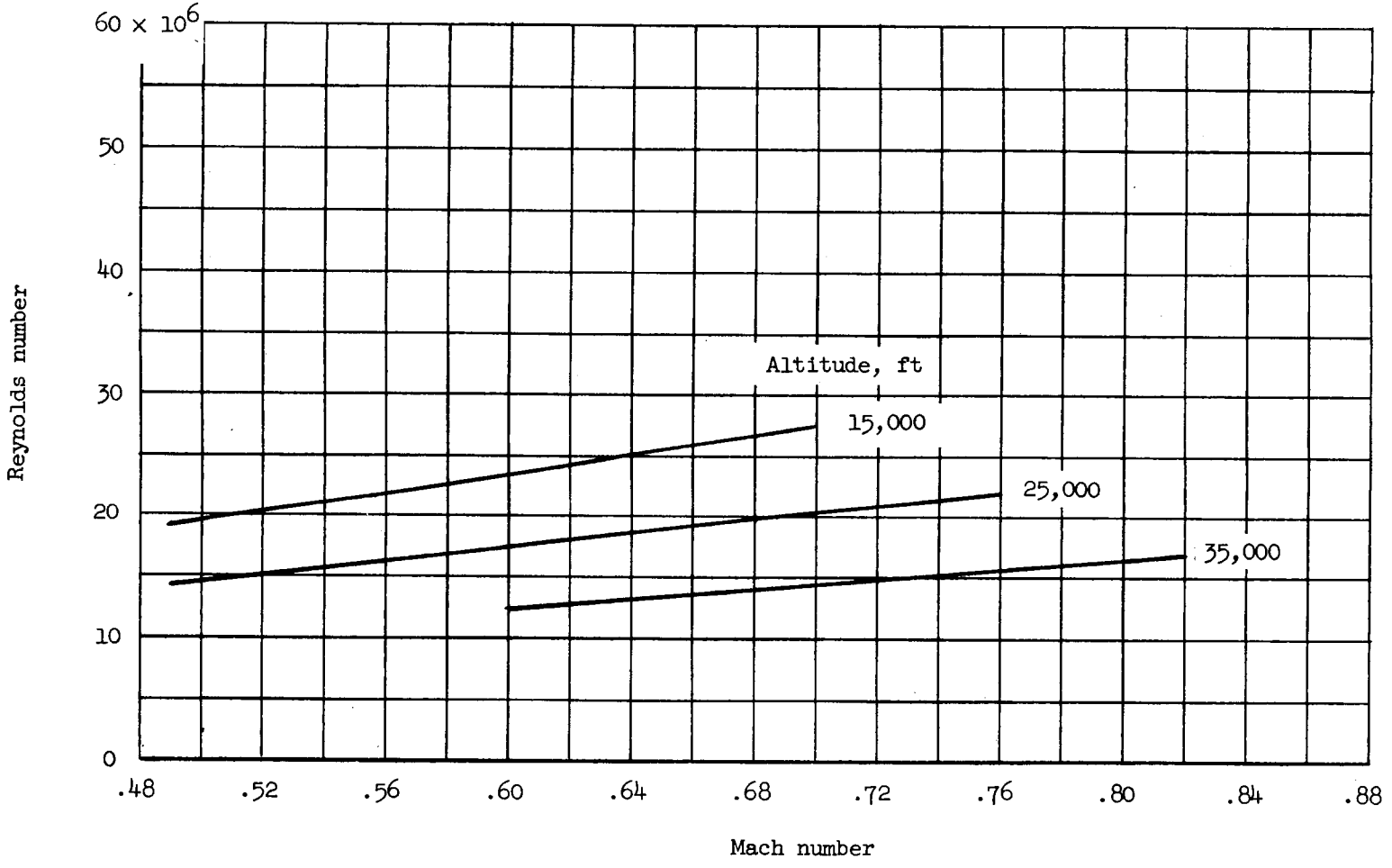

Figure 4.- Variation of Reynolds number with Mach number at the three test altitudes. Reynolds number based on $\bar{c}_h$.

Figure 5.- Positive directions of various quantities.

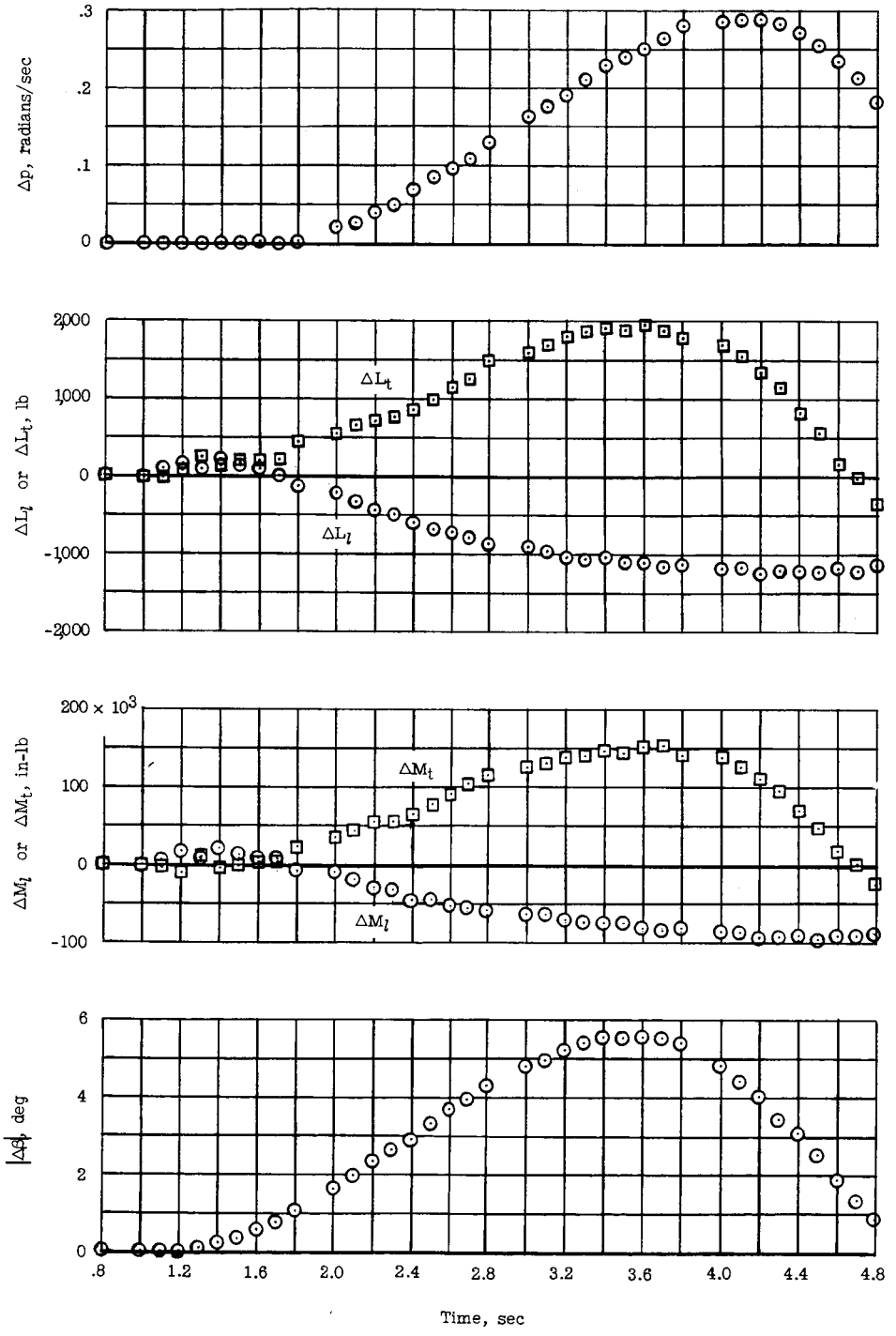

Figure 6.- Time histories from a typical right-rudder-step maneuver. Flight 24, run 22.

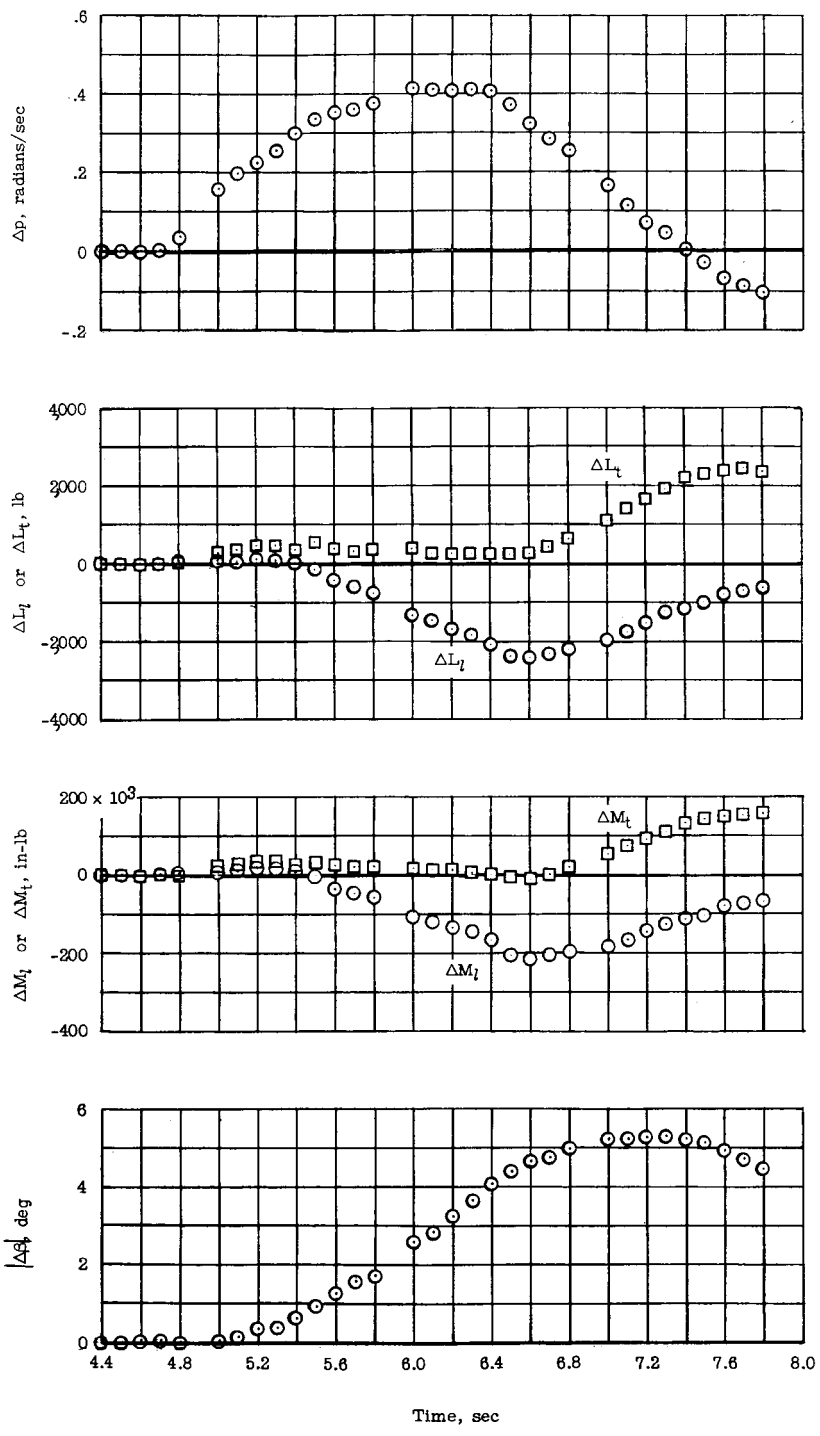

Figure 7.- Time histories from a typical right-aileron roll maneuver. Flight 24, run 21.

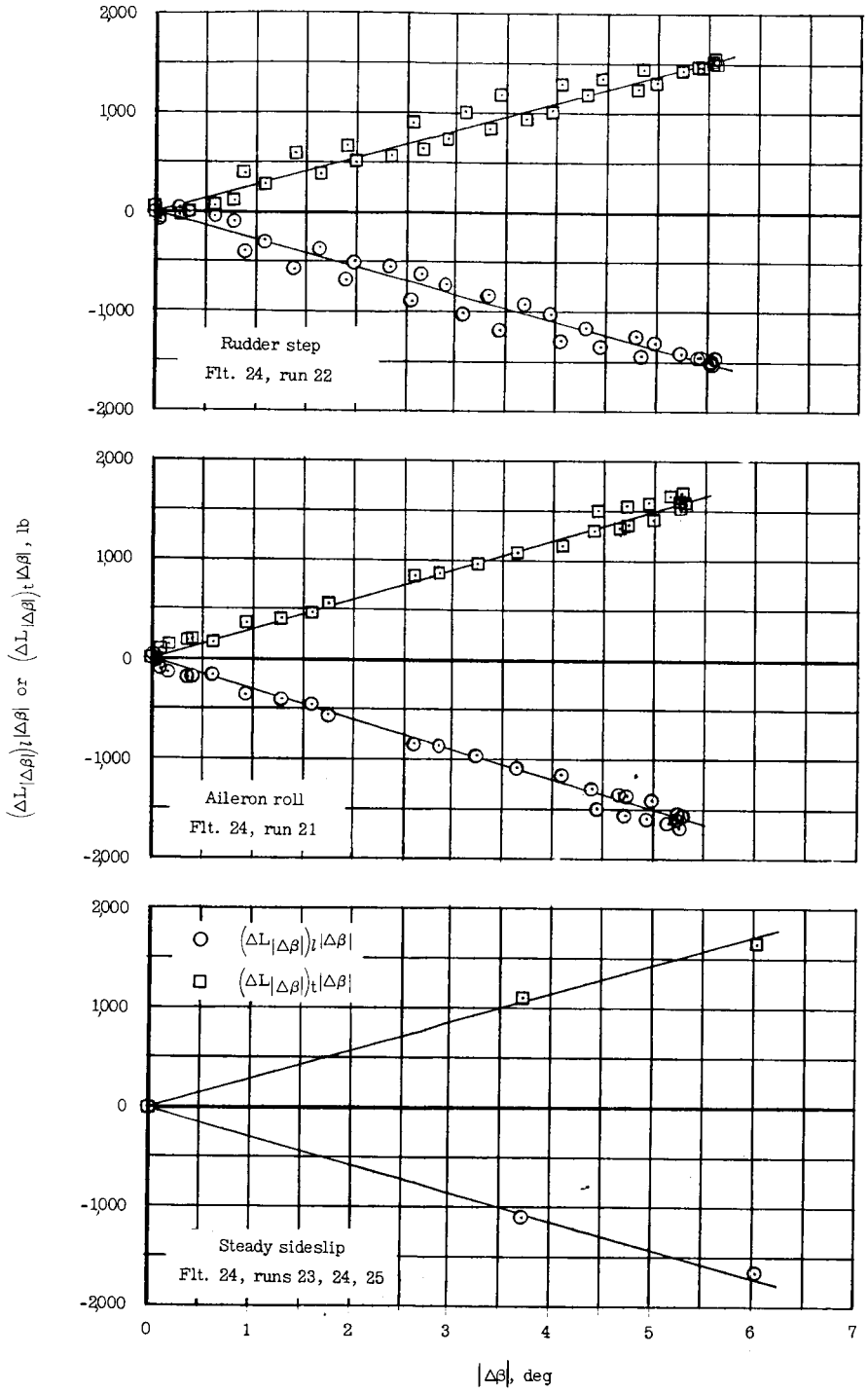

Figure 8.- Incremental horizontal-tail shear loads due to sideslip angle for typical test maneuvers.

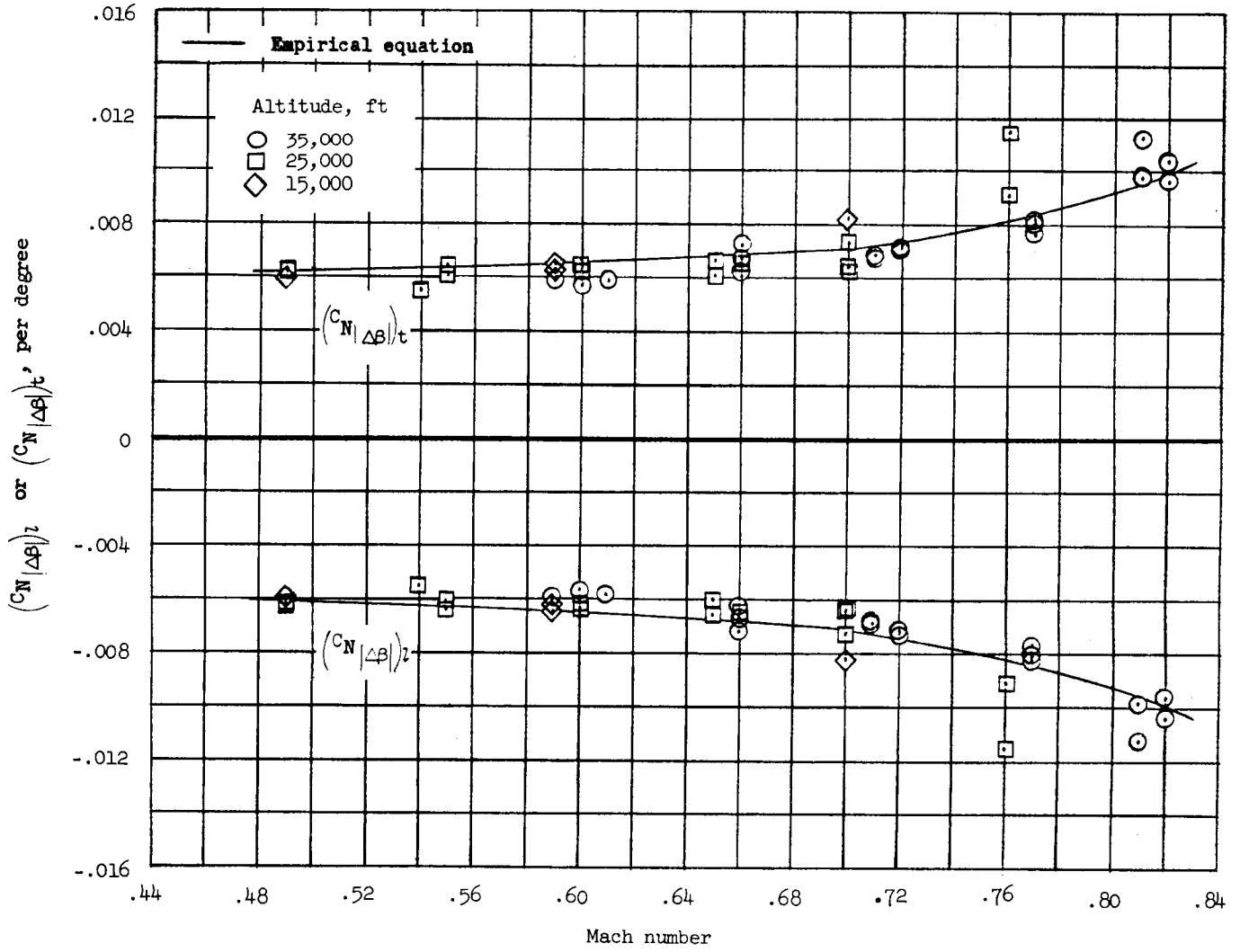

Figure 9.- Derivatives of the horizontal-tail normal force coefficient with respect to sideslip angle.

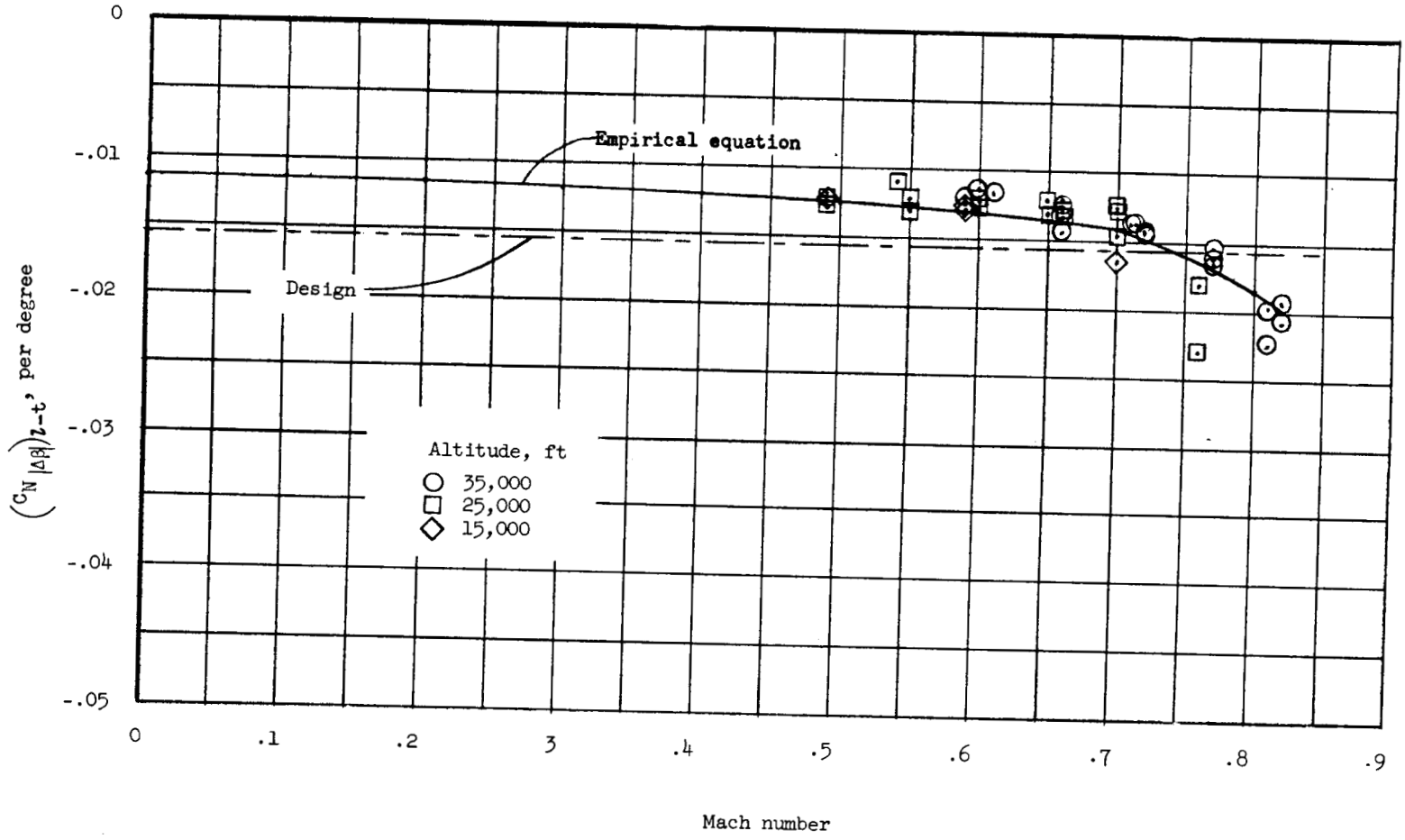

Figure 10.- Derivatives of the horizontal-tail unsymmetrical normal-force coefficient with respect to sideslip angle.

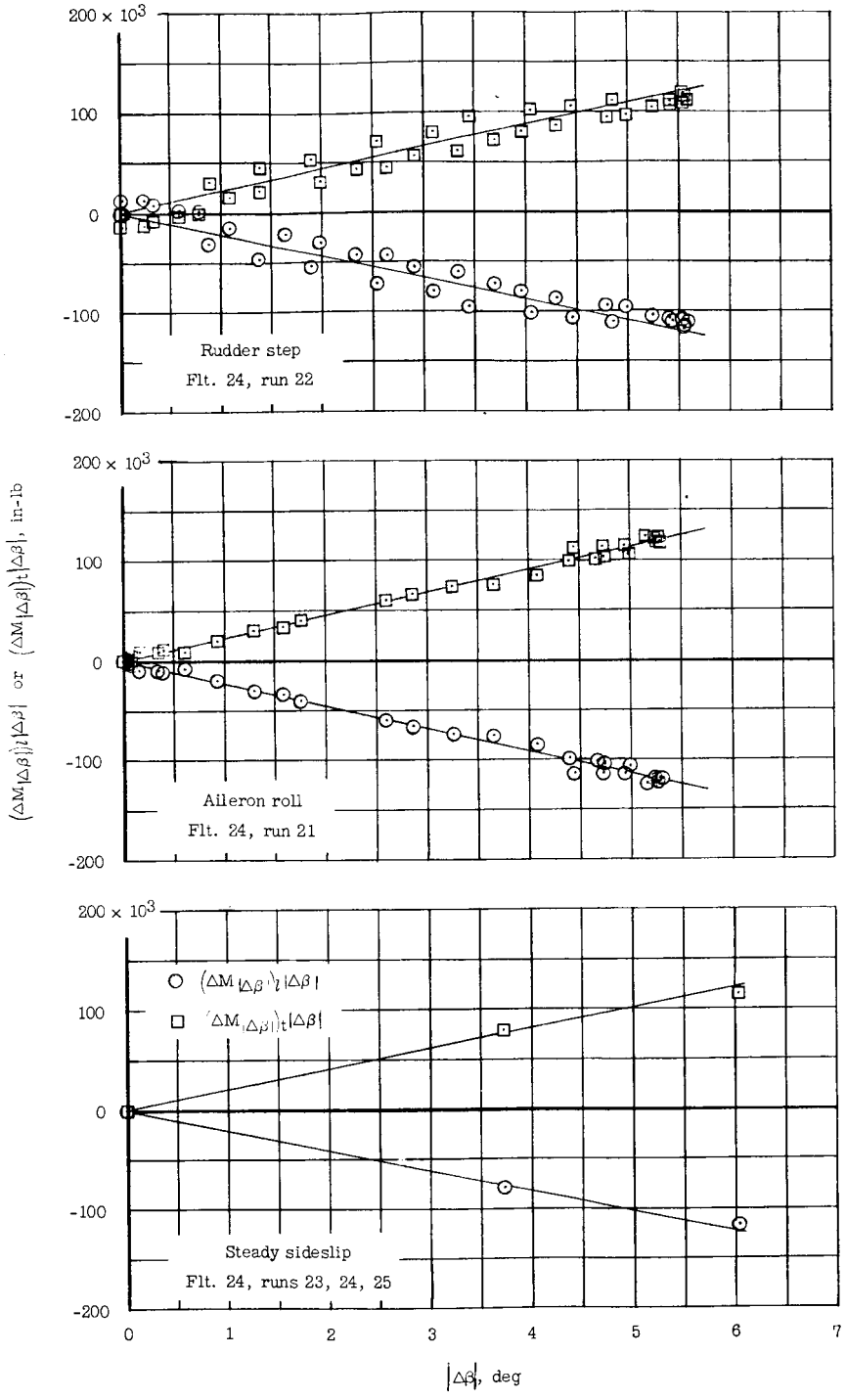

Figure 11.- Incremental horizontal-tail rolling moments due to sideslip angle for typical test maneuvers.

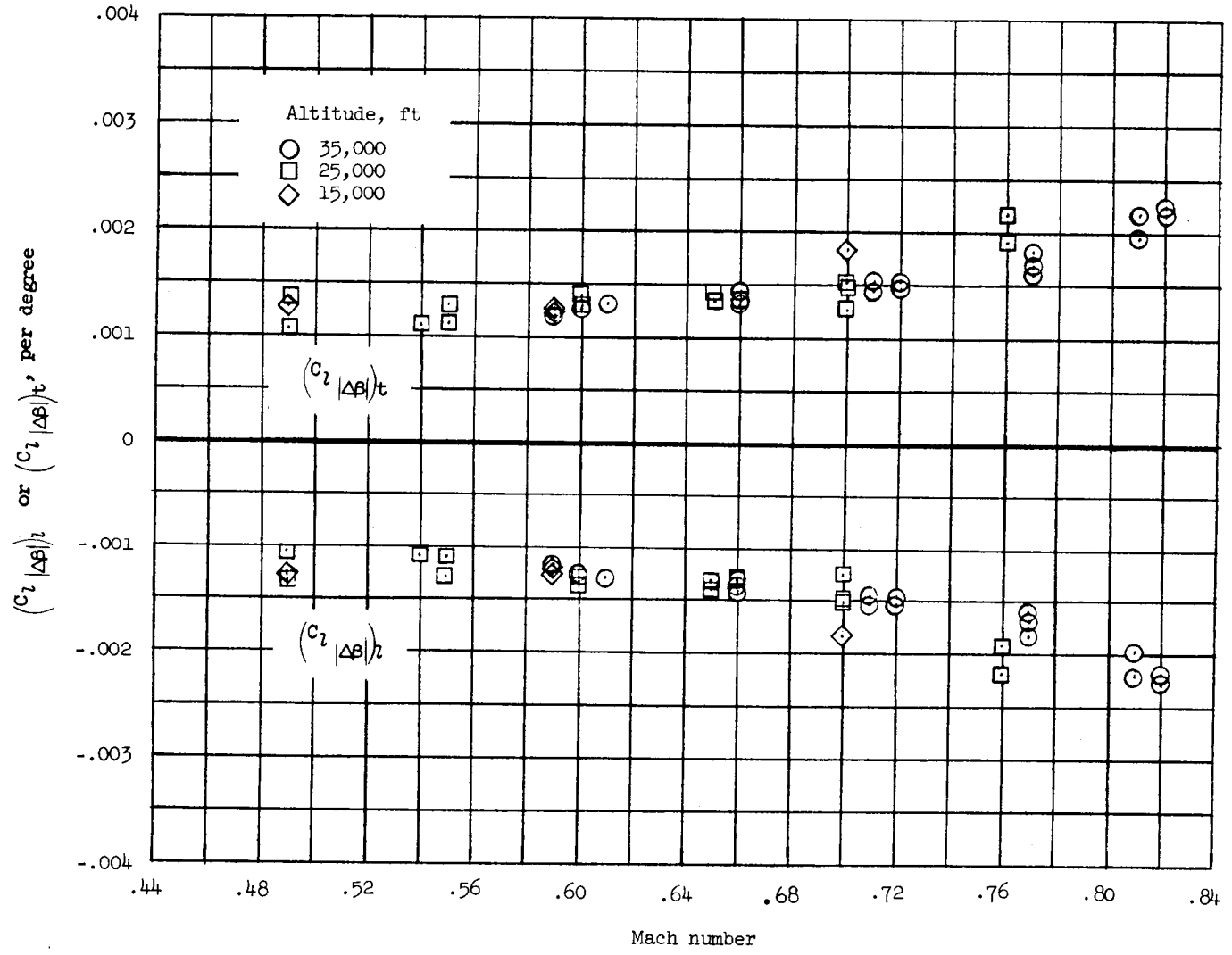

Figure 12.- Derivatives of the horizontal-tail rolling-moment coefficient with respect to sideslip angle.

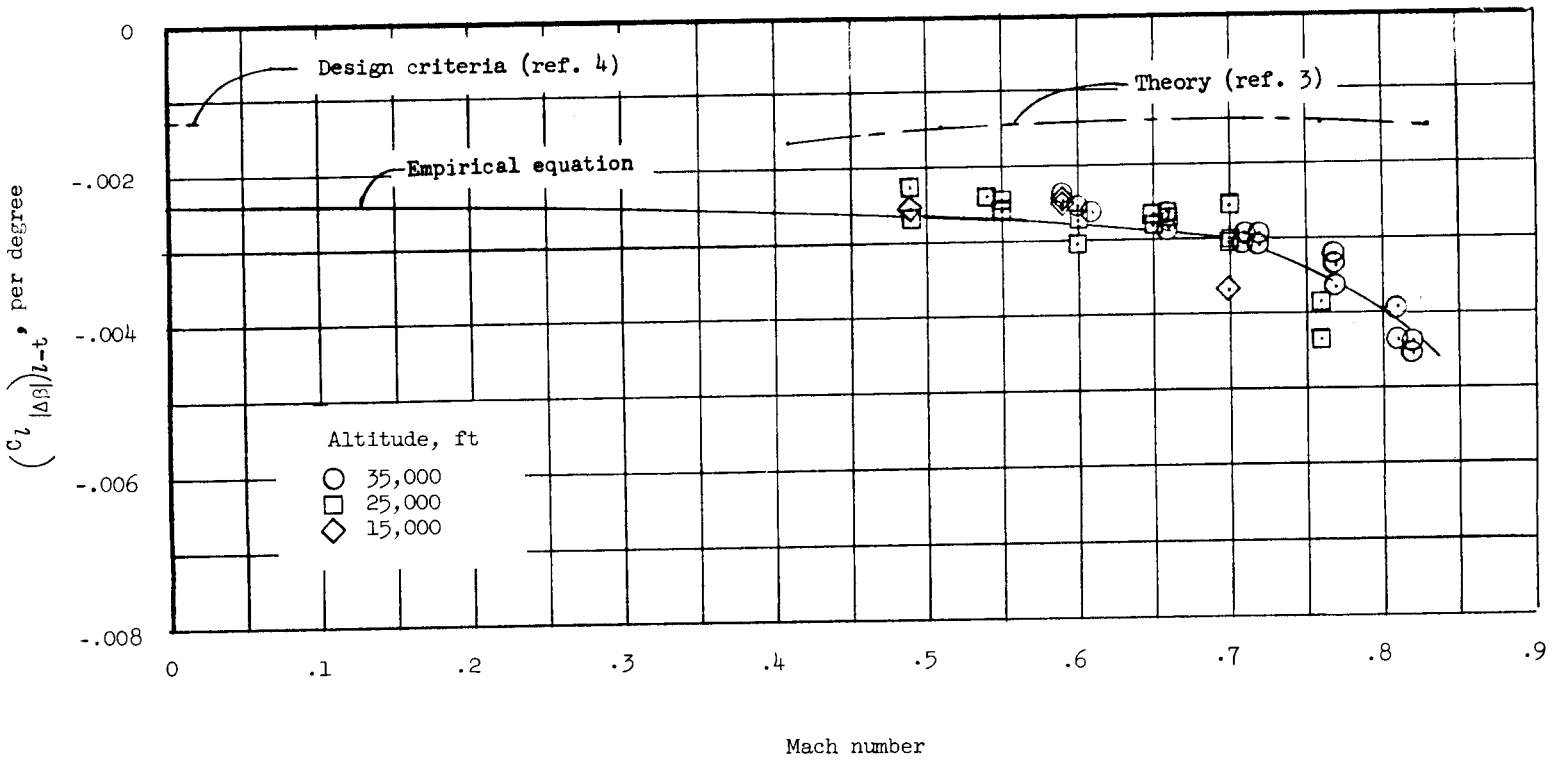

Figure 13.- Derivatives of the total horizontal-tail rolling-moment coefficient with respect to sideslip angle.

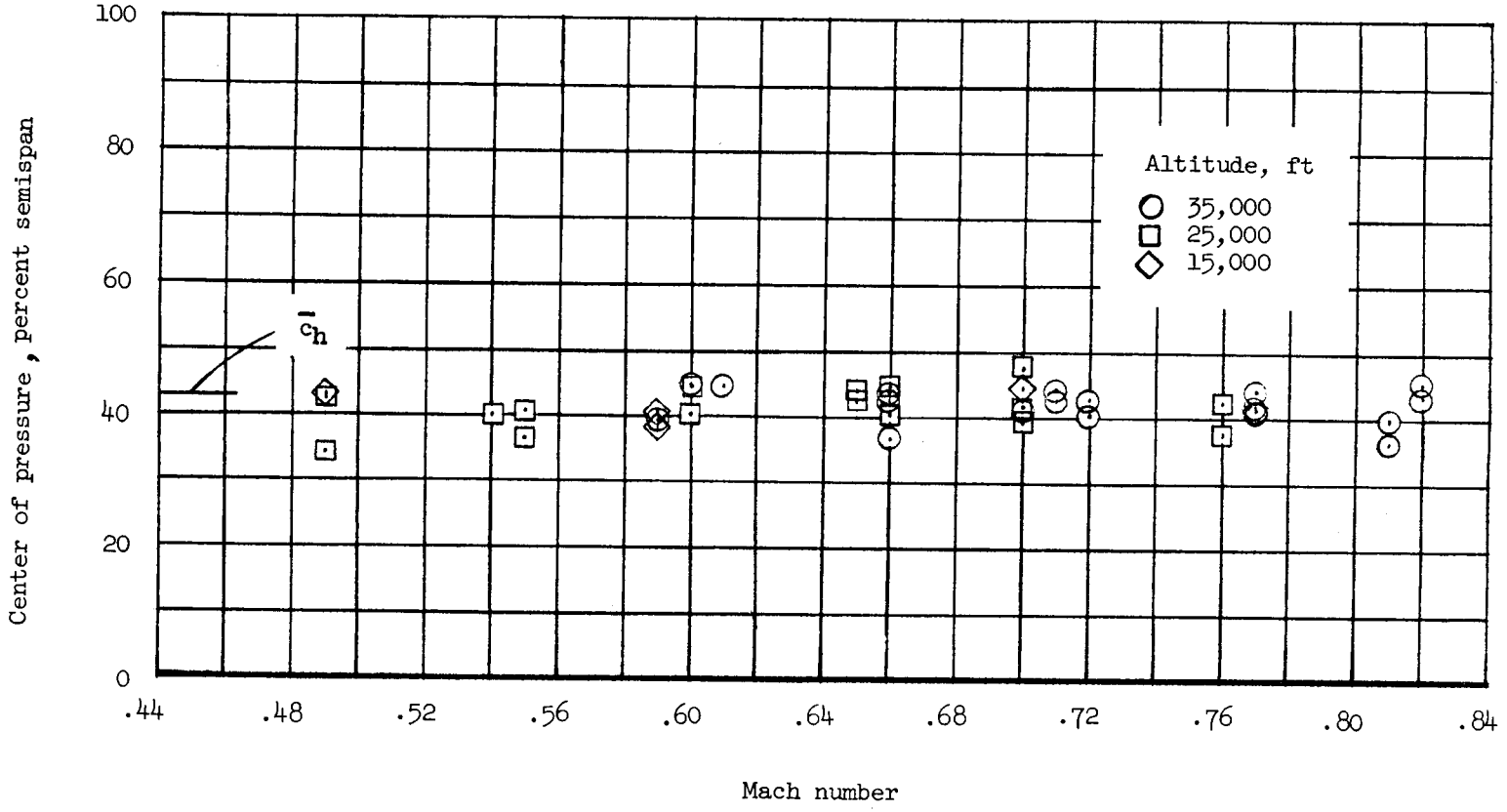

Figure 14.- Spanwise center-of-pressure locations of incremental loads due to sideslip angle on the leading or trailing horizontal tail.

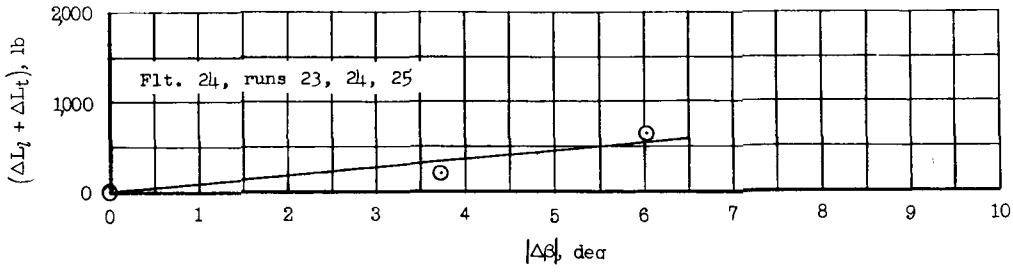

Figure 15.- Total incremental horizontal-tail loads measured during a typical series of steady sideslips.

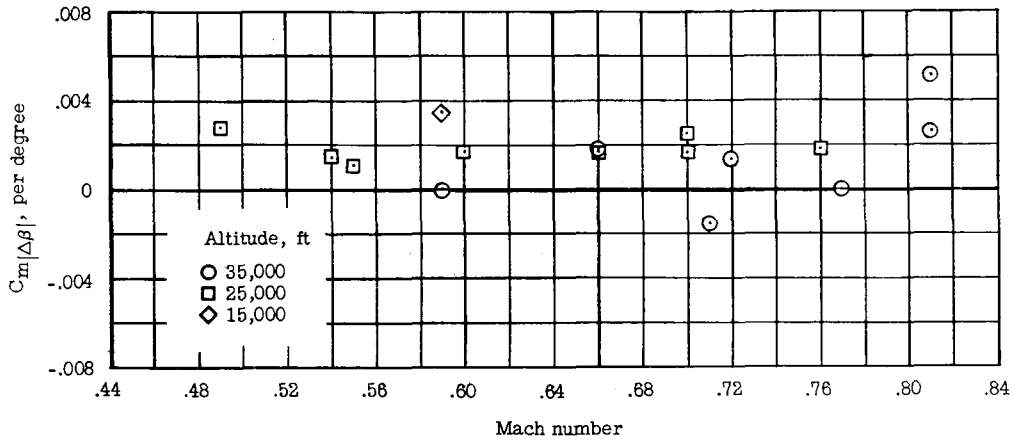

Figure 16.- Variation with Mach number of the derivatives of the wing-fuselage pitching-moment coefficient with respect to sideslip angle.

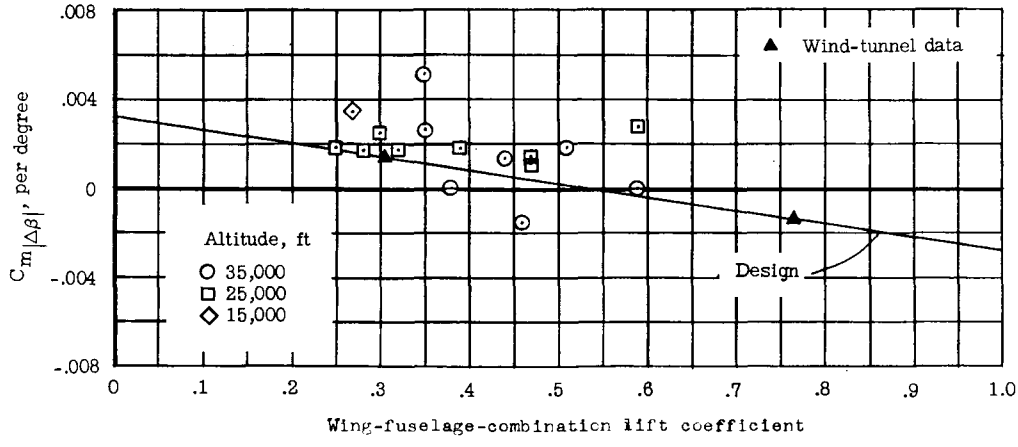

Figure 17.- Variation with wing-fuselage combination lift coefficient of the derivatives of the wing-fuselage pitching-moment coefficient with respect to sideslip angle.